

FIELD INVESTIGATION OF WAVE DISSIPATION OVER SALT MARSH VEGETATION DURING TROPICAL CYCLONE

Ranjit Jadhav^{1,2} and Qin Chen¹

Wave data were measured along a 28 m transect using 3 pressure transducers over a 2-day period during a tropical storm. The tropical storm force winds produced waves up to 0.4 m high (zero-moment) that propagated over vegetation of *Spartina alterniflora* submerged under a surge of over 1 m above the marsh floor. Measured wave heights, energy losses between gages and spectral energy dissipation models of rigid vegetation were utilized to estimate wave height decay rates, integral and frequency-dependent bulk drag coefficients, and frequency distribution of energy dissipation induced by the vegetation. Measurements showed that incident waves attenuated exponentially over the vegetation. The exponential wave height decay rate decreased as Reynolds number increased. The swell was observed to decay at a slower rate than the wind sea regardless of the wave height. The linear spatial wave height reduction rate increased from 1.5% to 4% /m as incident wave height decreased. The bulk drag coefficient estimated from the field measurement decreased with increasing Reynolds and Keulegan-Carpenter numbers. The energy dissipation varied across the frequency scales with the largest magnitude observed near the spectral peaks, above which the dissipation gradually decreased. The wave energy dissipation did not linearly follow the incident energy, and the degree of non-linearity varied with the frequency. For a given spectrum, the frequency-distributed drag coefficient increased gradually up to the peak frequency and remained approximately at a stable value at the higher frequencies. This spectral variation was parameterized by introducing a frequency-dependent velocity attenuation parameter inside the canopy. The spectral drag coefficient is shown to predict the distribution of energy dissipation with more accuracy than the integral coefficients, which results in a more accurate prediction of the mean wave period and spectral width of a wave field with vegetation.

Keywords: salt marsh; vegetation; bulk drag coefficient; random waves; wave attenuation; energy dissipation; tropical cyclone

INTRODUCTION

Coastal wetland vegetation serves as a natural defense system against storm surge and waves along many coastal regions of the world and is utilized to augment the structural protection measures for mitigation of coastal flooding. (e.g., Dixon et al. 1998, Lopez 2009, Gedan et al. 2011, Borsje et al. 2011, CPRA 2012). Waves lose energy by interacting with the obstructing vegetation resulting in wave height attenuation. Several existing studies have quantified reduction rates of integral wave heights and estimated bulk drag coefficients, and proposed theoretical models for energy dissipation (Dalrymple et al. 1984, Mendez and Losada 2004, Kobayashi et al. 1993, Chen and Zhao 2012) in a laboratory setting (Dubi and Tørum 1996, Løvås and Tørum 2001, Augustin et al. 2009, and Stratigaki et al. 2011) and in field conditions (Möller et al. 1999, Möller and Spencer 2002, Cooper 2005, Möller 2006, Bradley and Houser 2009, Riffe et al. 2011, Jadhav and Chen 2012). Recent studies have noted the importance of stem motion of flexible vegetation, and have proposed models that account for it (Bradley and Houser 2009, Mullarney and Henderson 2010, Riffe et al. 2011). Summaries of these studies can be found in Irish et al. (2008), Anderson et al. (2011), and Jadhav and Chen (2012). In spite of the fairly large number of studies, with the exception of Möller and Spencer (2002), all these studies have been carried out in a low-energy environment. Although challenging, there is a need to measure storm-induced waves in coastal wetlands (Smith et al. 2011). Additionally, except for Lowe et al. (2005, 2007), all of the previous studies primarily focused on the attenuation of integral wave parameters. Lowe et al. (2005) developed an analytical model to predict the magnitude of the in-canopy velocity of monochromatic waves propagating over a model canopy of rigid cylinders. Velocity attenuation inside the canopy was found to be dominantly dependent on the wave excursion length. Further extension of this model to random waves predicted preferential dissipation of high frequency waves inside the model canopy (Lowe et al. 2007). Apart from illustrations by Bradley and Houser (2009) and Paul and Amos (2011), there have been no reported studies that examine in detail the frequency-based characteristics of wave energy dissipation and drag coefficient in case of natural vegetation.

In this paper, we present and analyze field data on wave attenuation by coastal marshes in a high-energy environment produced by a tropical storm. Using measured wave records, we quantify the rates of wave attenuation, vegetation induced bulk drag coefficient, and wave height decay rate. We also identify spectral variation of the vegetation drag coefficient and present a method to determine it based

¹ Department of Civil and Environmental Engineering, and Center for Computation and Technology, Louisiana State University, 3418 Patrick F. Taylor Hall - LSU, Baton Rouge, LA 70803, USA.

² FTN Associates, 10508 North Glenstone Place, Baton Rouge, LA 70810, USA.

on an integral bulk drag coefficient and the velocity attenuation parameter. We hypothesize that the frequency-varying drag coefficient will predict spectral distribution of energy dissipation more accurately than an integral drag coefficient. To test the hypothesis, a new method is developed to parameterize the spectral drag coefficient over the entire range of measured wave spectra. The spectral and integral drag coefficients are then both used to estimate energy losses, and these estimates are compared to the observed dissipation to assess the validity of the parameterization and hypothesis.

DATA AND METHODS

Study Area and Experimental Setup

Three wave gages (pressure transducers) were deployed on a wetland with salt marsh vegetation in Terrebonne Bay (Louisiana) on the northern coast of the Gulf of Mexico (Figure 1). The bottom-mounted gages sampled continuously at 10 Hz covering Tropical Storm Lee (September 3-4, 2011). The Bay is a shallow (1-3 m), micro-tidal (tidal range < 0.5 m) estuary bordered by an intermittent chain of low-lying barrier islands to the south. The study site experiences shallow (≈ 0.1 m) flooding with diurnal tides but is prone to significant flooding during the passage of tropical storms and winter storms, which is an important feature of the regional meteorology.

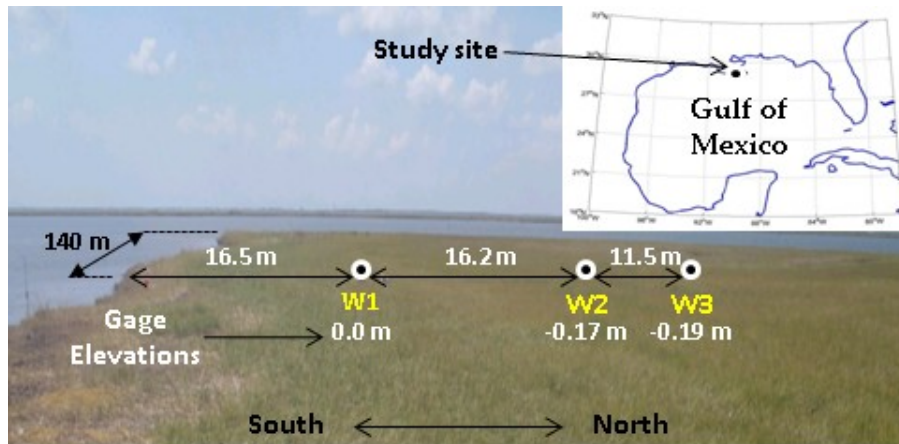


Figure 1. Study area location (Terrebonne Bay, Louisiana) and the schematic of experimental set up showing wave gages (W1, W2 and W3). Gage elevations shown are relative to gage W1. Not to scale.

The salt marsh vegetation primarily consisted of *Spartina alterniflora*. The plant is characterized by a thick (average diameter, measured at one-fourth the stem height of 8.0 mm) stem (average stem height, length between the plant base and the location of the topmost blade along the stem of 0.22 m) and thin, flexible narrow blades. The average stem population density was 422 stems/ m^2 , and the Young's Modulus was, $E_v = 80$ MPa ($E_v I_v = 0.015$ N·m 2) where $E_v I_v$ is the flexural rigidity and I_v is the second moment of inertia of a stem. The average total plant height was 0.63 m, defined as the length between the plant base and the tip of the plant with all blades aligned along the stem. Using the Euler-Bernoulli beam theory, the Young's Modulus was calculated by measuring the force required to bend the stem in the field by a known angle. Based on our field observations and the estimated non-dimensional stiffness parameter (Mullarney and Henderson 2010), the vegetation is treated as rigid (see analysis in Jadhav and Chen 2012).

The time series of continuous pressure measurement from the wave gauges were analyzed using standard spectral methods. The resulting energy spectra had bandwidth of 0.01 Hz, with 95% of the spectral energy between 0.03 Hz (low-frequency cutoff) and 0.7 Hz (high-frequency cutoff). The following definitions of the integral wave parameters are used: significant wave height, $H_{mo} = 4\sqrt{m_0}$; mean wave period, $T_z = \sqrt{m_0/m_2}$; and spectral width, $\nu = (m_0 m_2 / m_1^2 - 1)$ where m_0 , m_1 , and m_2 are the zero-th, first and second moment of the wave spectrum, respectively.

Measured Wave Conditions

The wave records consisted of a low-energy offshore swell (7-10 s) and locally generated, storm-induced seas (2-4.5 s). The tropical storm produced a surge of about 0.8 m (average water depth, $h=0.55$ m) on the marsh which otherwise experiences only shallow flooding due to diurnal tides. The significant wave heights (H_{mo}) on the marsh (Gage W1) correspondingly increased up to 0.4 m (average 0.22 m) with peak wave periods of 2.5-4.5 s. The average relative wave height (H_{mo}/h) at W1 was 0.41, which reduced to 0.12 at W3. The average spectral width, ν , increased from 0.51 at W1 to 0.53 at W3, indicating broad spectra. Note that we analyzed only those wave records that were collected when water depth was greater than 0.4 m, as the wave energy levels were insignificant for depths smaller than 0.4 m.

Wave Height Attenuation

We quantified wave height reduction due to vegetation per unit length of the wave propagation as follows (e.g., Möller 2006, Bradley and Hauser 2009, Lövstedt and Larson 2010).

$$r = \frac{H - H_o}{H_o} \cdot 100 \quad (1)$$

where H_o is the incoming and H is the outgoing wave height along the measurement transect of length Δx .

Wave height attenuation has also been characterized as an exponential decay process (Asano et al. 1993, Kobayashi et al. 1993, Möller et al. 1999, Cox et al. 2003) expressed as,

$$H = H_o e^{-k_H x} \quad (2)$$

where k_H is the decay rate and x is the distance along the direction of wave propagation from the location of the first or windward gage (where H_o is measured) to the location where H is sought.

Energy Dissipation Model

Assuming the linear wave theory holds, the wave energy balance equation for waves propagating through vegetation is written as follows,

$$\frac{\partial E C_g}{\partial x} = -S_v \quad (3)$$

where, $E = (1/8)H^2$ is the wave energy density, H is the wave height, $C_g = nc$ is the group velocity, $c = \sqrt{(g/k)\tanh(kh)}$ is the phase speed, k is the wave number, h is the still water depth, g is the acceleration due to gravity, and coefficient n is given by $n = (1/2)[1 + (2kh/\sinh 2kh)]$. The cross-shore coordinate is represented by x , and S_v is the time averaged rate of energy dissipation due to vegetation per unit horizontal area. This balance equation assumes that the wave energy loss due to vegetation is dominant compared to the other source terms. To ascertain the validity of this assumption, the relative magnitude of source terms for the local wave generation and the losses due to bottom-friction, white-capping, and depth-limited breaking were evaluated. The wave records with significant potential for the magnitude of these source terms to be dominant were removed from further analysis (for details see Jadhav and Chen 2012).

To estimate wave energy losses caused by vegetation, we treat stems as rigid obstructing cylindrical elements that impart drag forces on the flow (e.g., Dalrymple et al. 1984, Kobayashi et al. 1993, Mendez and Losada 2004). In this paper, we employ the model proposed by Chen and Zhao (2012) which was reorganized in Jadhav et al. (2012) with the introduction of a normalized velocity attenuation parameter, α_n . In this model the wave energy dissipation, S_v , is expressed as follows.

$$\langle S_v \rangle = \int S_{ds,v}(\sigma) d\sigma \quad (4)$$

where,

$$S_{ds,v}(\sigma) = \frac{1}{2} \frac{\bar{C}_D b_v N_v}{g} \alpha_n^2(\sigma) \left(\frac{\sigma}{\sinh kh} \right)^2 \left(\int_{-h}^{-(h-sh)} U_{rms}(z) \cosh^2[k(h+z)] dz \right) S_e(\sigma) \quad (5)$$

and

$$U_{rms}(z) = \sqrt{2 \int \frac{\sigma^2 \cosh^2 k(h+z)}{\sinh^2 kh} S_e(\sigma) d\sigma} \quad (6)$$

where \bar{C}_D is the spectrally-averaged, or integral, drag coefficient, b_v is the stem diameter, N_v is the vegetation population density, σ is the wave angular frequency, s is the ratio of vegetation height, h_v , to the still water depth, h , and U_{rms} is the root-mean-squared (RMS) velocity, z is the vertical coordinate with origin at the still water level and pointing upwards, and S_e is the spectral energy density. The velocity attenuation parameter is defined as the ratio of the vegetation-affected velocity to the velocity in the absence of vegetation at a given elevation inside the canopy.

The spectrally variable drag coefficient is then expressed as,

$$C_D(\sigma) = \bar{C}_D \cdot \alpha_n^2(\sigma) \quad (7)$$

RESULTS

Observed Wave Height Attenuation

The wave heights reduced rapidly in the first reach (W1-W2) compared to the second reach (W2-W3). The mean incident RMS wave heights of 0.09 m to 0.24 m reduced to 0.02-0.09 m within the study transect. The percentage wave height reduction rate, r , (Eq. (1)) decreased from 4% to 1.5% /m, with increasing wave height. Note that the wave height was directly proportional to the water depth.

The exponential wave height decay was also quantified by determining decay rates (k_H) obtained by fitting Eq. (2) to the set of simultaneous RMS wave heights recorded at gages W1, W2, and W3. The exponential decay rates, k_H ranged from 0.022 to 0.051 /m ($R^2 > 0.98$). Existing literature reports decay rates of 0.011 /m (random waves over artificial kelp in a laboratory flume, Dubi and Tørum 1996), 0.015-0.101 /m (monochromatic waves over artificial vegetation in a laboratory flume, Kobayashi et al. 1993) and 0.007-0.015 /m (random waves in the seagrass, Bradley and Houser 2009). As shown in Figure 2, the k_H was found to vary with the Reynolds number, R_e ($= \rho b_v u_b / \mu$), and Keulegan-Carpenter number, K_C ($= u_b T_z / b_v$), where u_b ($= H_{rms} \omega_z / 2 \sinh k_z h$) is the maximum near-bed orbital velocity in the absence of vegetation given by the linear wave theory using the measurements at the seaward of the two bounding gages. The subscript z indicates the mean value of the parameter.

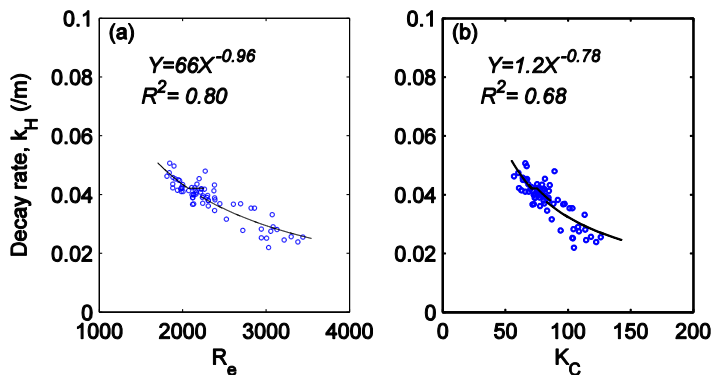


Figure 2. Variation of exponential wave height decay rate with Reynolds number, and Keulegan-Carpenter number. Independent variables are based on measurements at gage W1.

Observed Frequency Distribution of Wave Energy Dissipation

Reduction in the wave height of a random wave field is a result of wave energy dissipation across the frequency scales. Figure 3 shows frequency distribution of energy dissipation of one measured wave record. The magnitude of energy dissipation is higher at the frequencies adjacent to the spectral peak.

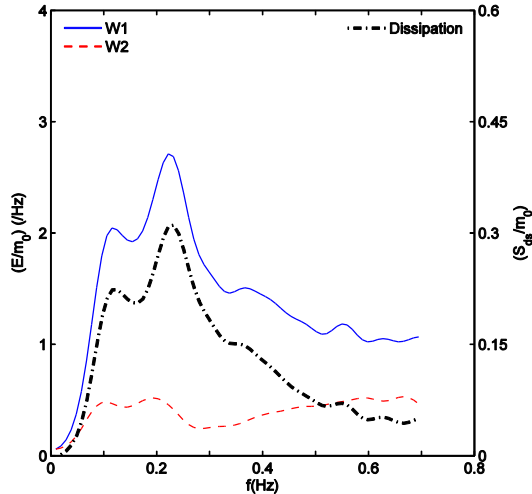


Figure 3. Normalized energy density and energy dissipation spectrum in reach W1-W2 recorded on September 3, 2011 at 3:45 UTC. Spectra normalized by the zero-th moment (m_0) of the energy spectrum measured at W1.

The distribution of energy dissipation is generally assumed to follow the incident wave energy density spectrum linearly (e.g., Suzuki et al. 2011). We assessed the validity of this assumption, by testing the following hypothesis and using our measurements:

$$S_{ds}(f) = a \cdot E(f)^b \quad (8)$$

where a and b are determined by regression analysis. The exponent b is a measure of linearity (linear when $b=1$) of this relationship.

For each incident energy spectrum, $E(f)$, and the corresponding dissipation spectrum, $S_{ds}(f)$, Eq. (8) was fitted across three frequency bands, namely swell (0.03-0.16 Hz), wind-sea (0.16-0.32 Hz) and the high frequency (0.32-0.7 Hz) band. Thus, for each spectrum, three coefficient pairs (a, b) were obtained, one for each band. Figure 4 shows a fitting example for one wave record.

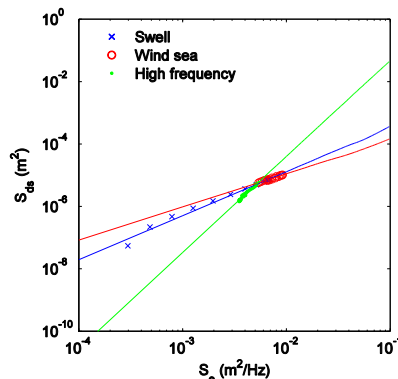


Figure 4. Variation of wave energy dissipation with respect to incident energy density recorded on September 3, 2011 at 3:45 UTC

Coefficient pairs were determined for all measured wave records and the data with R^2 (coefficient of determination) less than 0.8, were excluded from the analysis. Table 1 shows the mean values of b for the three frequency bands considering all wave records. The wave records are divided into three ranges of K_C signifying three ranges of hydrodynamic conditions.

Table 1. Mean values of exponent b in Eq. (8) considering all wave records			
Frequency band	K_C Range		
	$K_C \leq 47$	$47 < K_C \leq 83$	$K_C > 83$
Swell	1.9	1.6	1.5
Sea	1.3	1.2	1.2
High Frequency	1.0	2.0	2.6

It was observed that, the relationship tended to be most linear in the wind-sea band across the entire range of K_C numbers and slightly more nonlinear in the swell frequency band. The degree of non-linearity was found to increase at smaller K_C numbers (which are more common in the second reach, W2-W3). In the high frequency band ($f > 0.32$ Hz) the relationship is linear for waves with $K_C < 47$, and gradually becomes nonlinear with increasing K_C number. Note that the energy spectra and hence, the energy dissipation, in this high frequency range is also affected by the noise amplification and non-linear triad interactions. The coefficient a was verified to be equal to the ratio, $\int E^b df / \int S_{ds} df$ for all wave records.

Integral and Frequency-Dependent Bulk Drag Coefficients

The bulk drag coefficients were estimated by applying the Chen and Zhao (2012) model. The left hand side of Eq. (3) was calculated by dividing the difference of measured wave energy flux between adjacent pairs of wave gages (i.e., W1-W2 and W2-W3) by the distance between them. The right hand side was calculated by using Eq. (4) by numerical integration along the vertical stem height and along the spectral frequency. Figure 5 shows the estimated values of bulk drag coefficients, \bar{C}_D , plotted against the Keulegan-Carpenter (K_C) number resulting in the following regression equation,

$$\bar{C}_D = 70 K_C^{-0.86} \quad 25 < K_C < 135 \quad (9)$$

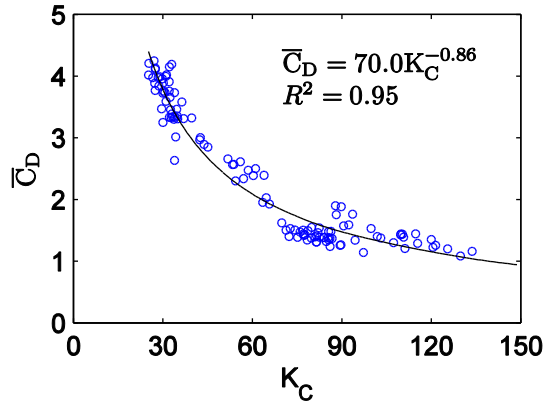


Figure 5. Estimated integral bulk drag coefficient and its variation with the Keulegan-Carpenter number.

The K_C number is based on the wave parameters measured at the seaward gage of the bounding gages. Also, \bar{C}_D represents the “bulk” value of the drag coefficient over the vegetation transect, rather than the drag coefficient of an idealized, isolated, cylinder (see e.g., Tanino and Nepf 2008).

Using the form suggested by Tanino and Nepf (2008), the coefficients, \bar{C}_D , is related to the Reynolds number, R_e , as follows,

$$\bar{C}_D = 2 \left(\frac{1300}{R_e} + 0.18 \right) \quad 600 < R_e < 3,200 \quad (10)$$

If the bulk drag coefficient is treated as a function of frequency, then Eq. (5) can also be used to estimate frequency distributed drag coefficient using measured energy dissipation. Such estimates for several wave records are shown in Figure 6. It can be seen that a single integral drag coefficient value over the entire spectral frequency scale does not adequately represent spectral variation of the drag coefficient.

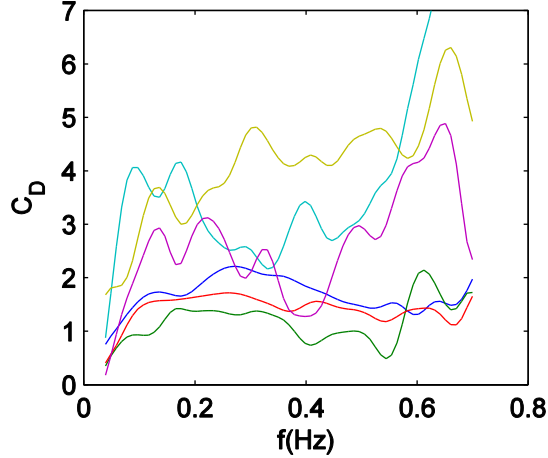


Figure 6. Estimated spectral bulk drag coefficients for six different wave records.

As a predictive tool, Eq. (7) can be used to compute the frequency varying drag coefficient, C_D , when \bar{C}_D and α_n are known. For a given spectrum (with its K_C), \bar{C}_D can be determined using Eq. (9). To calculate α_n , the following procedure was followed. Using the measured energy spectra, Eq. (3) and Eq. (4) were numerically solved to compute $f - \alpha_n$ profile for each spectrum. All such profiles were then ensemble-averaged, resulting in the single $\bar{\alpha}_n$ curve shown in Figure 7. The $\bar{\alpha}_n$ values increase from the lower frequencies to the peak frequency region, followed by a slight decrease in the frequencies above peak. In our analysis, the $\bar{\alpha}_n$ values for frequencies above about 0.4 Hz are considered unreliable, due to the influence of non-linear energy transfer, and greater amplification of noise resulting from the pressure response function at those frequencies.

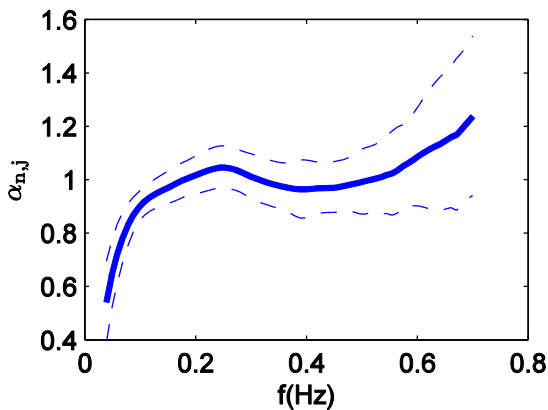


Figure 7. Spectral variation of ensemble-averaged velocity attenuation parameter, α_n , based on all 118 measured profiles. Dashed lines represent ± 1 standard deviation.

Prediction of Energy Dissipation using Estimated Drag Coefficients

Here we compare energy dissipation predicted by using integral (\bar{C}_D) and spectral (C_D) drag coefficients. For a single wave record, first, a K_C value is calculated and then \bar{C}_D is determined from Eq. (9). For the same record, the spectral C_D is determined by using Eq. (7) and Figure 7. Spectral dissipation is then calculated using Eq. (5). Figure 8 shows comparison plots of the measured and predicted energy dissipation using these two approaches, for one wave record.

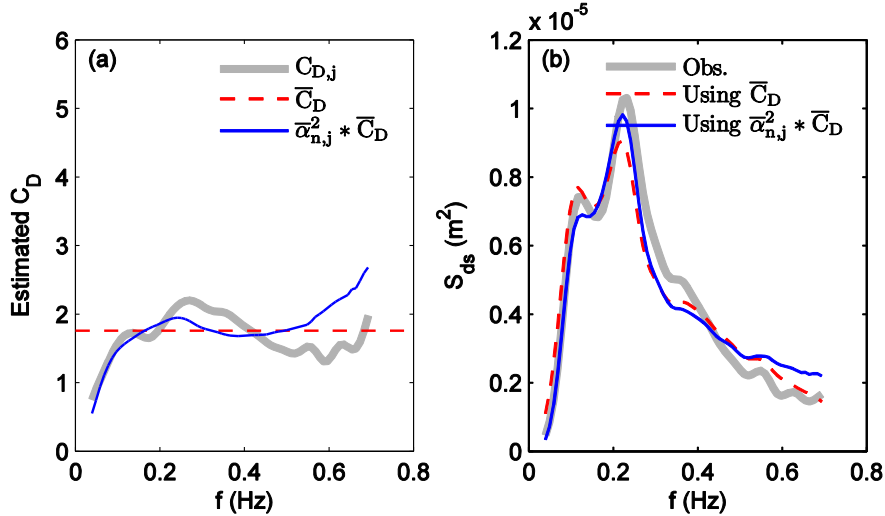


Figure 8. Comparison of observed and predicted spectral energy dissipation between W1 and W2 using average and spectral drag coefficient for a sample wave record on September 3, 2011 at 3:45 UTC. (a) Estimated C_D (b) Dissipation.

The frequency-dependent C_D is seen to predict the frequency distribution of energy dissipation with better accuracy than the integral \bar{C}_D . In the frequency range with the dominant energy (0.03-0.36 Hz), the energy dissipation predicted by the frequency varying C_D has much less error (not shown in the figure) than that predicted by the integral \bar{C}_D . The real potential of the C_D method over the \bar{C}_D method is reflected in the improved prediction of the integral parameters that are governed by the distribution of energy dissipation. For example, the absolute error in the estimate of mean period at gage W2 reduced from 9.0% (\bar{C}_D method) to 4.1% (C_D method) on average over the entire data set. Similar improvement was observed in the estimates of the spectral width (Figure 9). On average, the absolute error reduced from 25.1% to 5.4% and from 9.2% to 2.1% at gages W2 and W3, respectively.

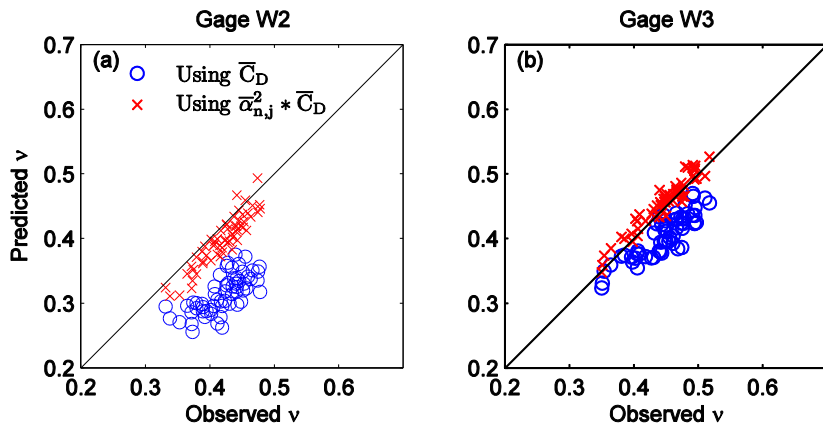


Figure 9. Scatter plots of observed and predicted spectral widths by the two methods. (a) For all spectra measured at W2. (b) For all spectra measured at W3.

SUMMARY AND CONCLUSIONS

The paper presents a field data set on attenuation of wave heights and frequency-dependent characteristics of energy dissipation of random waves over salt marsh (*Spartina alterniflora*). The data set is unique as it was collected under the tropical storm generated, high-energy waves. Most of the existing field studies have been carried out in the low-energy environment.

Wave spectra were obtained from measured waves over salt marsh vegetation to study vegetation induced energy dissipation along a marsh transect with two reaches. The waves in the leading reach of the transect were more energetic, highly nonlinear, occurred in shallower water, and exhibited greater energy dissipation compared to the subsequent reach, where waves were less energetic, significantly less nonlinear, and exhibited less energy dissipation.

The measured wave height reduction rate decreased from 4% to 1.5 % /m as the wave height increased (commensurate with the water depth). Although it offers a compact way, such a reduction rate is an unreliable general indicator of the effectiveness of vegetation in wave damping because it depends on vegetation types and wave conditions. Consistent with the previous studies, the storm waves were observed to decay exponentially over vegetation. The decay rates reduced from 0.051 /m to 0.022 /m with increasing Reynolds number and Keulegan-Carpenter number.

The wave energy dissipation was observed to be frequency-dependent with the greatest energy dissipation measured at the spectral peak frequencies. Further, it did not follow the incident energy density linearly. The relationship of the spectral dissipation to energy density was less nonlinear in the wind-sea than the swell band, and became slightly more nonlinear and consistent for larger waves. The estimated integral bulk drag coefficient decreased from 4.3 to 1.2 with increasing Reynolds number (600-3200) and Keulegan-Carpenter number (25-135). The drag coefficient was also observed to be frequency-dependent. It increased gradually up to the spectral peak and then remained more or less uniform. A normalized velocity attenuation parameter, α_n , is introduced to parameterize the frequency-distributed drag coefficient. The frequency-distributed drag coefficient is shown to improve the prediction accuracy of the spectral energy distribution, which consequently improves the accuracy of a number of parameters, such as mean wave period and spectral width.

It should be noted that the drag coefficient parameterization presented in this paper has been verified using the same dataset on which it is based. While it validates the parameterization, it needs to be further tested as more independent datasets become available.

ACKNOWLEDGMENTS

The study was supported by the US Department of Homeland Security (DHS) through the Southeast Region Research Initiative (SERRI) and by the US National Science Foundation (NSF) (Grant No. CBET-0652859 and DMS-1115527). We thank T. Baker Smith, LLC for logistical support and topographic surveying, and the Louisiana Universities Marine Consortium (LUMCON) for providing meteorological data. Graduate students Kyle Parker, James Chatagnier and James Bouanchaud assisted in the field study. We also thank Dr. Jane Smith of ERDC-USAE and Dr. Weiming Wu of the University of Mississippi for helpful discussions. Any opinions, findings, conclusions and recommendations expressed in this paper are those of the authors and do not necessarily reflect the views of the NSF or the DHS.

REFERENCES

- Anderson, M. E., J. M. Smith, and S. K. McKay. 2011. Wave Dissipation by Vegetation. *Coastal and Hydraulics Engineering Technical Note ERDC/CHL CHETN-I-82*. U.S. Army Engineer Research and Development Center, Vicksburg, MS.
- Asano, T., H. Deguchi, and N. Kobayashi. 1993. Interaction between water wave and vegetation, in *Proceedings of 23rd International Conference on Coastal Engineering*, pp. 2710–2723, ASCE, New York, NY.
- Augustin, L. N., J. L. Irish, and P. J. Lynett. 2009. Laboratory and numerical studies of wave damping by emergent and near-emergent wetland vegetation, *Coastal Eng.*, 56, 332–340.
- Bendat, J. S., and A. G. Piersol. 2000. *Random data: analysis and measurement procedures*, John Wiley and Sons, Inc. New York, NY.

- Borsje, B. W., B. K. van Wesenbeeck, F. Dekker, P. Paalvast, T. J. Bourma, M. M. van Katwijk, and M. B. de Vries. 2011. How ecological engineering can serve in coastal protection, *Ecol. Eng.* 37 (2), 113–122.
- Bradley, K., and C. Houser. 2009. Relative velocity of seagrass blades: Implications for wave attenuation in low energy environments, *J. Geophys. Res.*, 114, F01004, doi:10.1029/2007JF000951.
- Chen, Q., and H. Zhao. 2012. Theoretical models for wave energy dissipation caused by vegetation, *J. Engineering Mech.*, 138(2), 221-229.
- Cox, R., S. Wallace, and R. Thomson. 2003. Wave damping by seagrass meadows, in *Proceedings of 6th International COPEDEC Conference*. Lanka Hydraulic Institute, Colombo, Sri Lanka, Paper No 115.
- CPRA. 2012. Louisiana's Comprehensive Master Plan for a Sustainable Coast. Coastal Protection and Restoration Authority of Louisiana. Baton Rouge, LA.
- Dalyrmple, R. A., J. T. Kirby, and P. A. Hwang. 1984. Wave refraction due to areas of energy dissipation, *J. Waterw. Port Coastal Ocean Eng.*, 110, 67–79.
- Dixon, A. M., D. J. Leggett, and R. C. Weight. 1998. Habitat creation opportunities for landward coastal re-alignment: Essex case study. *J. Chartered Institution of Water and Environmental Management*, 12, 107–112.
- Dubi, A., and A. Tørum. 1996. Wave energy dissipation in kelp vegetation, in *Proceedings of the 25th International Conference on Coastal Engineering*, pp. 2626-2639, ASCE, New York, NY.
- Gedan, K. B., M. L. Kirwan, E. Wolanski, E. B. Barbier, and B. R. Silliman. 2011. The present and future role of coastal wetland vegetation in protecting shorelines: an answering recent challenges to the paradigm. *Climatic Change*, 106, 7-29.
- Irish, J. L., L N. Augustin, G. E. Balsmeier, and J. M. Kaihatu. 2008. Wave dynamics in coastal wetlands: a state-of-knowledge review with emphasis on wetland functionality for storm damage reduction, *Shore and Beach*, 76, 52–56.
- Jadhav, R.S., and Q. Chen. 2012. Wave attenuation by salt marsh vegetation during tropical cyclone, *J. Geophys. Res.*, submitted.
- Jadhav, R.S., Q. Chen., and J.M. Smith. 2012. Spectral distribution of wave energy dissipation by salt marsh vegetation, *Coastal Eng.*, submitted.
- Kobayashi, N., A. W. Raichlen, and T. Asano. 1993. Wave attenuation by vegetation, *J. Waterw. Port Coastal Ocean Eng.*, 119, 30–48.
- Lopez, J.A. 2009. The Multiple Lines of Defense Strategy to Sustain Coastal Louisiana, *J. Coastal Res.*: Special Issue 54 - Geologic and Environmental Dynamics of the Pontchartrain Basin [FitzGerald & Reed]: pp. 186 – 197.
- Løvås, S.M., and A. Tørum. 2001. Effect of kelp *Laminaria hyperborea* upon sand dune erosion and water particle velocities, *Coastal Eng.*, 44, 37–63.
- Lövstedt, C.B., and M. Larson. 2010. Wave damping in reed: Field measurements and mathematical modeling. *J. Hyd. Eng.*, 136(4), 222-233.
- Lowe, R. J., J. R. Koseff, and S. G. Monismith. 2005. Oscillatory flow through submerged canopies: 1. Velocity structure, *J. Geophys. Res.*, 110, C10016, doi:10.1029/2004JC002788.
- Lowe, R., J. Falter, J. Koseff, S. Monismith, and M. Atkinson. 2007. Spectral wave flow attenuation within submerged canopies: Implications for wave energy dissipation, *J. Geophys. Res.*, 112, C05018, doi:10.1029/2006JC003605.
- Mendez, F. J., and I. J. Losada. 2004. An empirical model to estimate the propagation of random breaking and non-breaking waves over vegetation fields, *Coastal Eng.*, 51, 103–118.
- Möller, I., T. Spencer, J. R. French, D. Leggett, and M. Dixon. 1999. Wave transformation over salt marshes: a field and numerical modelling study from North Norfolk, England, *Estuarine Coastal Shelf Sci.*, 49, 411–426.
- Möller, I., and T. Spencer. 2002. Wave dissipation over macro-tidal salt marshes: effects of marsh edge typology and vegetation change, *J. Coast. Res.*, SI36, 506–521.
- Möller, I. 2006. Quantifying salt marsh vegetation and its effect on wave height dissipation: results from a UK East coast saltmarsh, *Estuarine Coastal Shelf Sci.*, 69, 337–351.
- Mullarney, J.C., and S.M. Henderson. 2010. Wave forced motion of submerged single stem vegetation, *J. Geophys. Res.*, 115, C12061, doi:10.1029/2010JC006448.
- Paul, M., and C. L. Amos. 2011. Spatial and seasonal variation in wave attenuation over *Zostera noltii*, *J. Geophys. Res.*, 116, C08019, doi:10.1029/2010JC006797.

- Riffe, K. C., S. M. Henderson, and J. C. Mullarney. 2011. Wave dissipation by flexible vegetation, *Geophys. Res. Lett.*, 38, L18607, 5 pp., doi:10.1029/2011GL048773
- Smith, J. M., R. E. Jensen, A. B. Kennedy, J. C. Dietrich, and J. J. Westerink. 2011. Waves in wetlands: Hurricane Gustav, in *Proceedings of the 32nd International Conference on Coastal Engineering*.
- Stratigaki, V., E. Manca, P. Prinos, I. J. Losada, J. L. Lara, M. Sclavo, C. L. Amos, I. Cáceres and A. Sánchez-Arcilla. 2011. Large-scale experiments on wave propagation over *Posidonia oceanica*, *J. Hydraulic Res.*, 49, sup1, 31-43.
- Suzuki, T., M. Zijlema, B. Burger, M. C. Meijer, and S. Narayan. 2011. Wave dissipation by vegetation with layer schematization in SWAN, *Coastal Eng.*, 59, 64-71.
- Tanino, Y., and Nepf, H. M. 2008. Laboratory investigation of mean drag in a random array of rigid, emergent cylinders, *J. Hydraul. Eng.*, 134, 1, 34-41.